pH-dependent structural transitions of Alzheimer amyloid peptides

Paul E. Fraser,* Jack T. Nguyen,* Witold K. Surewicz,‡ and Daniel A. Kirschner*
*Neurology Research, Children's Hospital, and Department of Neurology, Harvard Medical School, Boston Massachusetts 02115; and ‡National Research Council, Division of Chemistry, Ottawa, Ontario, Canada

ABSTRACT To understand the molecular interactions leading to the assembly of β/A4 protein into the hallmark fibrils of Alzheimer's disease (AD), we have examined the ability of synthetic peptides that correspond to the β/A4 extracellular sequence to form fibrils over the range of pH 3–10. Peptides included the sequences 1–28, 19–28, 17–28, 15–28, 13–28, 11–28, and 9–28 of β/A4. The model fibrils were compared with isolated amyloid with respect to morphology, conformation, tinctorial properties, and stability under denaturing conditions. Electron microscopy, Fourier-transform infrared (FT-IR) spectroscopy, and x-ray diffraction revealed that the ionization states of the amino acid sidechains appeared to be a crucial feature in fibril formation. This was reflected by the ability of several peptides to undergo fibril assembly and disassembly as a function of pH. Comparisons between different β/A4 sequences demonstrated that the fibrillar structure representative of AD amyloid was dependent upon electrostatic interactions, likely involving His-13 and Asp-23, and hydrophobic interactions between uncharged sidechains contained within residues 17–21. The results also indicated an exclusively β-sheet conformation for the synthetic (and possibly AD fibrils) in contrast to certain other (e.g., systemic) amyloids.

INTRODUCTION

Proteinaceous fibrils contained within senile plaques and neurofibrillary tangles (NFT) are distinguishing neuropathological features of Alzheimer's disease (AD) (Selkoe, 1989). Whereas a combination of several constituents including microtubule-associated protein tau (Kosik et al., 1986; Wischik et al., 1988), ubiquitin (Mori et al., 1987), and neurofilament proteins (Anderton et al., 1982) are closely associated in the intraneuronal NFT paired helical filaments, a single 39–42 residue protein, β/A4, is the predominant component of the extracellular AD amyloid (Glenner and Wong, 1984*a*, 1984*b*; Masters et al., 1985*a*). Cloning has revealed that β/A4 is located toward the COOH-terminus of a 695-residue precursor protein (βAPP_{695}) (Kang et al., 1987). The alternate transcripts, βAPP_{751} and βAPP_{770}, which contain protease inhibitor inserts, have also been identified (Ponte et al., 1988; Tanzi et al., 1988; Kitaguchi et al., 1988). βAPP contains an extracellular NH_2-terminal domain, a single transmembrane domain, and a short cytoplasmic segment. The sequence of β/A4 includes the first 28 residues of the extracellular domain and 11–14 residues of the proposed transmembrane region. Proteolytic cleavage at or near position 612 of βAPP (Lys-16 of β/A4) results in the release of soluble secreted protein of undefined function (Palmert et al., 1989; Sisodia et al., 1990; Esch et al., 1990). The residual membrane-bound region of β/A4 may, however, play a key role in neuronal degeneration possibly via a receptor-mediated pathway (Yankner et al., 1990). These observations have led to proposals that incorrect processing resulting from defective constituent proteases (Sisodia et al., 1990; Esch et al., 1990) and/or via abnormal posttranslational modifications (Buxbaum et al., 1990) may be a factor in the production and accumulation of β/A4, and in AD etiology.

Recent immunocytochemical investigations (Spillantini et al., 1990*a*, 1990*b*) have suggested a multistep process in the continued proteolysis and final self assembly of the β/A4 fragment into amyloid fibrils. Several structural models for β/A4 and other amyloid proteins (e.g., systemic) have been proposed (Glenner et al., 1974; Turnell et al., 1986; Gorevic et al., 1987; Kirschner et al., 1987). Although there is considerable evidence that the amyloid proteins are folded into a β-sheet conformation, additional secondary structural elements such as α-helices may also contribute to fibril formation.

This study was undertaken to determine which residues are crucial to fibril formation and how certain interresidue interactions may underlie fibril stability. Examination by electron microscopy (EM), Fourier-transform infrared spectroscopy (FT-IR), and x-ray diffraction of a series of synthetic peptides corresponding to successively longer stretches of the β/A4 extracellular region have enabled us to identify residue-specific electrostatic and hydrophobic interactions necessary for

Address correspondence to Daniel A. Kirschner.

0006-3495/91/11/1190/12 $2.00

AD-like fibril formation. FT-IR analysis and x-ray diffraction of the synthetic fibrils suggests that the AD fibrils are most closely approximated by an all β-sheet model.

MATERIALS AND METHODS

Peptide synthesis

Amyloid peptide sequences (Fig. 1) used in this study [β-(19–28), β-(17–28), β-(15–28), β-(13–28), β-(11–28) and β-(9–28)] were purchased from Peninsula Laboratories (Belmont, CA) and Star Biochemicals (Torrance, CA). A purity of greater than 98% was verified by amino acid analysis and analytical HPLC. Proton NMR spectra (360 MHz) were also obtained (Francis Bitter Magnet Laboratory, Cambridge, MA) for each of the commercial peptides as an additional purity check by our laboratory. The spectra were consistent with the amino acid composition, and no extraneous or minor peaks (indicating truncated peptides) were observed. The full length extracellular portion of β-(1–28) was synthesized and purified using methods previously described (Kirschner et al., 1987; Fraser et al., 1991).

Electron microscopy

For thin sectioning, hydrated gels of the peptides (~30 mg/ml) were fixed by vapor diffusion for 2–3 h over 2.5% (vol/vol) buffered glutaraldehyde followed by 2–3 h postfixation by vapor diffusion with buffered OsO_4 (2% wt/vol). The samples were dehydrated through a graded ethanol series and embedded in Epon. Sections were counterstained with 3% (wt/vol) uranyl acetate and Reynold's lead citrate. For negative staining, carbon-coated Pioloform grids were floated on buffered aqueous solutions of the peptides (0.5–2 mg/ml) and stained with 2% (wt/vol) uranyl acetate or 2% (wt/vol) ammonium molybdate. The peptide assemblies were observed in a JEOL 100S operated at 80 kV or a JEOL 1200EX operated at 120 kV. Fibril dimensions were measured from electron micrographs and were calibrated using tropomyosin paracrystals kindly provided by Dr. C. Cohen (Brandeis University, Waltham, MA).

Effect of pH on fibrillar morphology was observed by dissolving lyophilized peptides in appropriately buffered solutions. The specific buffers are detailed in the figure legends. Fibrillar stability was also examined under denaturing conditions by mixing preformed fibrils (2 mg/ml) in a 1:1 ratio with 8 M urea. These solutions were left at room temperature for several days before negative staining to provide maximal opportunity for fibril dissolution.

Fourier-transform infrared spectroscopy

IR spectra were collected on a Digilab FTS-60 (Cambridge, MA) operated at 2 cm^{-1} resolution. Peptide solutions (5–20 mg/ml) were prepared in unbuffered D_2O and pH was adjusted by additions of NaOD or DCl. Electrode readings were uncorrected for deuterium effects. Sample aliquots (~10 μl) were placed in demountable cells containing CaF_2 windows separated by 50 μm teflon spacers. In some cases, the commercial peptides contained small amounts of trifluoroacetic acid (TFA) (used in HPLC purification) which gave an overlapping band at ~1670 cm^{-1}. In order to remove residual TFA, these peptides were additionally purified by chromatography on an Amberlite IR-45 minicolumn (Muga et al., 1990). In some cases the residual overlapping band was eliminated by subtraction from the final spectrum.

X-ray diffraction

Buffered peptide solutions (10–15 mg/ml) were slowly concentrated by air drying in siliconized thin walled glass capillaries (Charles Supper Co., Natick, MA). Final peptide concentration, estimated from the reduction in solution volume, was typically 50 mg/ml. Diffraction experiments were performed using nickel-filtered and double-mirror focused CuK_α radiation from an Elliot GX-20 rotating anode generator operated at 35 kV by 35 mA. Diffraction patterns were recorded on DEF film (Kodak) with exposure times of 1–3 d. The specimen to film distance, ~70 mm, was calibrated with known standards. Measurement of the spacings and intensities was carried out as previously described (Kirschner et al., 1987).

Congo red staining

Aliquots of each of the peptide solutions were air dried on glass slides and dehydrated for 20 min with 100% ethanol. The resulting films were stained with Congo red (5%; CR) in 80% ethanol saturated with NaCl. Excess CR was removed with three 10 min washes of 90% ethanol. The stained samples were examined between crossed polarizers to determine the presence or absence of the amyloid-associated green birefringence.

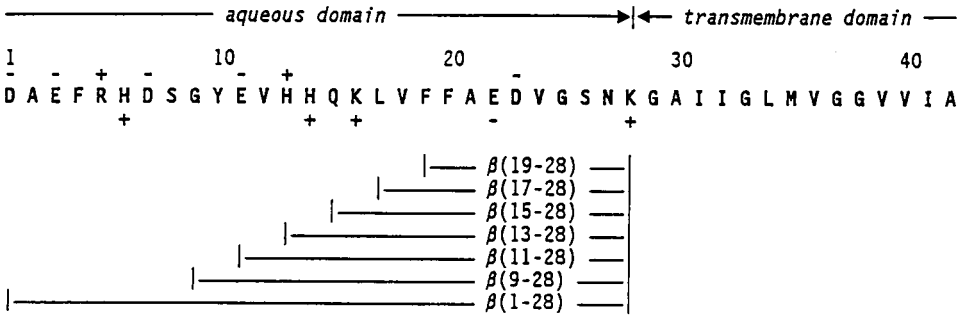

FIGURE 1 Sequence of β/A4 protein indicating the peptides examined in this study. The complete 1–42 segment encompassing both the extracellular and transmembrane regions corresponds to residues 597–638 of the βAPP (Kang et al., 1987). The charges of the various residues (+ or −) are positioned above and below the protein sequence consistent with the spatial orientation of the sidechains as would be found in an all β-conformation.

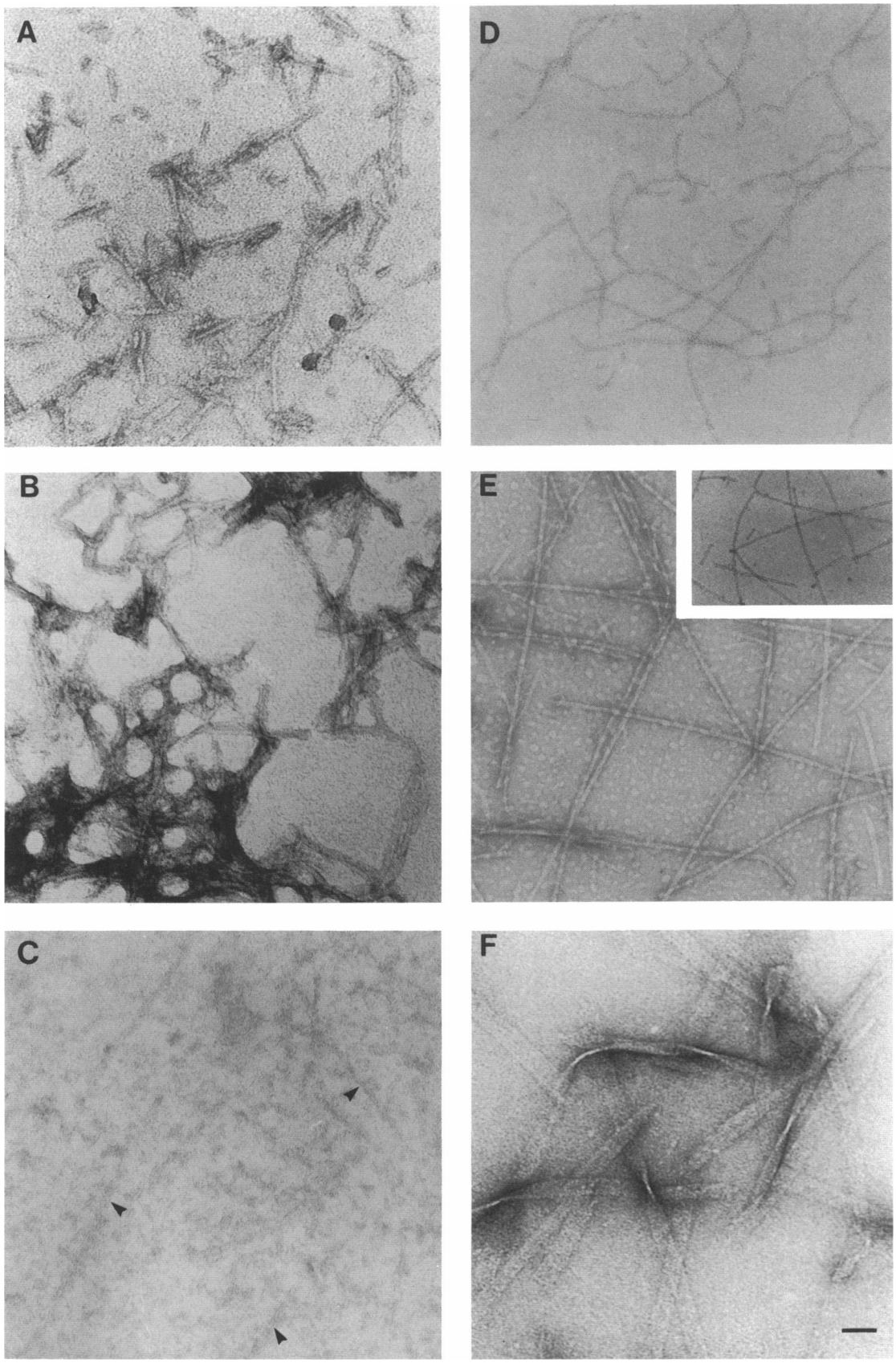
A
D
B
E
C
F

RESULTS AND INTERPRETATION

pH affected fibril formation and morphology

The extracellular β-(1–28) segment displayed a well defined pH dependence in forming stable fibrils (Fig. 2, *A–C*). At lower pH (2.5), 60–80 Å diameter fibrils were infrequently observed and appeared largely as fragments only several hundred Ångstroms in length. Raising the pH to 5.5 resulted in the appearance of numerous unbranched fibrils of similar diameters but much greater in length. At pH 8 such fibrils were mostly replaced by amorphous material with occasional lightly-stained fibrils.

The removal of eight residues (including several charges) from the NH_2-terminal to yield β-(9–28) changed not only the pH dependence of the peptide in forming fibrils but also the morphological characteristics of the fibrils (Fig. 2 *D–F*). At pH 2.0, the few fibrils that formed were poorly contrasted and ~35 Å in diameter. An increase to pH 4 produced a transition to long, unbranched fibrils 70–90 Å in diameter which remained unchanged up to pH 6–7. A further increase to pH 9 caused a transition in morphology to flexible, flattened ribbons, which were of indeterminate length and had dimensions of 200–225 Å by 50–55 Å. Above pH 9 no recognizable fibrillar or ribbon-like assemblies were obtained.

Peptides β-(11–28) and β-(13–28) exhibited identical pH dependence as β-(9–28), i.e., small indistinct fibrils at pH 2 followed by the formation of regular amyloid-like fibrils over the pH range 3–7 and eventually the formation of extended ribbons or slabs at pH 9.

As native AD amyloid is characteristically insoluble (Masters et al., 1985*a*), the stability of the in vitro amyloid-like β(9–28), β-(11–28), and β-(13–28) fibrils (pH 7) was tested under denaturing conditions. Each peptide maintained a fibrillar, amyloid morphology in 4 M urea but tended to be shorter than untreated fibrils (Fig. 2 *E*; *inset*).

The deletion of His-13 and His-14 to produce β-(15–28) altered not only the pH range at which fibrils could be formed but also their morphology (Fig. 3, *A* and *B*). Unlike the above longer peptides, β-(15–28) initially formed numerous 45–50 Å diameter fibrils at pH 2.5–3. With time, these fibrils apparently polymerized and formed 175–300 Å by 35–40 Å ribbons. From approximately pH 3–6, a mixture of ribbon structures and unbranched amyloid-like 75–90 Å diameter fibrils were observed. Further increases in pH resulted in the formation of predominantly amyloid-like fibrils. At pH > 9 no fibrils were formed.

Peptide β-(17–28) formed assemblies in the same pH range as β-(15–28), but the morphological characteristics were different (Fig. 3, *C* and *D*). At pH 2 the peptide formed extensive ribbons 1,200–1,500 Å in width. These ribbons tended to aggregate into large bundles which stacked edgewise on the Pioloform support to reveal individual thicknesses of 55–60 Å. Increasing to pH 6 produced a number of similar large ribbon structures that were accompanied by some shorter fibrillar fragments. High ionic strength (500 mM NaCl) reversed the fragmentation such that only extensive flat sheets with widths up to 3,500 Å were observed. These structures did not fold or twist, and were of indeterminate thickness. Fragmented β-(17–28) ribbons were observed at pH 9, and amorphous structures at pH > 10. Increasing the ionic strength with other peptides [e.g., β-(11–28)] did not alter the fibril morphology but did cause an increased lateral aggregation (data not shown).

β-(19–28), the smallest peptide examined, differed from β-(17–28) by only Phe-17 and Phe-18; however, fibrillar assemblies were formed only at pH < 3 and at greatly increased peptide concentrations (~25 mg/ml). The β-(19–28) assemblies appeared as long, occasionally twisted unbranched fibrils 90–110 Å in diameter (Fig. 4). These fibrils were very labile and had to be stained in an ethanol-based (50% by vol) uranyl acetate solution to avoid disruption. The formation of ribbon structures similar to those seen with β-(17–28) have been reported (Gorevic et al., 1987), but we have not confirmed these observations.

Globular substructure of model amyloid fibrils revealed in thin section

Oblique sections of fibrils revealed 25–30 Å 'globular' subunits (Fig. 5 *A*) resembling those found in fibrils of native AD (Miyakawa et al., 1986) and systemic amyloid (Cohen et al., 1982). In some cases the individual subunits appeared organized in staggered arrays to suggest a slight helical twisting (*arrowheads*, Fig. 5 *A*). Well defined longitudinal sections (Fig. 5, *B* and *C*)

FIGURE 2 Electron micrographs of negative-stained preparations of β-(1–28) at (*A*) pH 2.5 (20 mM glycine); (*B*) pH 5.5 (20 mM HEPES); and (*C*) pH 8.0 (20 mM Tris). Arrowheads in (*C*) indicate the lightly-contrasted fibrils. Morphological transitions of β-(9–28) from (*D*) narrow filaments at pH 2.0 (20 mM glycine), to (*E*) amyloid-like fibrils at pH 6 (20 mM HEPES), and eventually to (*F*) ribbons at pH 9 (20 mM Tris). (*E*, *inset*) β-(13–28) assemblies in 4 M urea, pH 6.2. Peptide concentrations were typically 0.5–2.0 mg/ml. Scale bar, 500 Å; inset in *E* has been reduced 2.5-fold with respect to other panels.

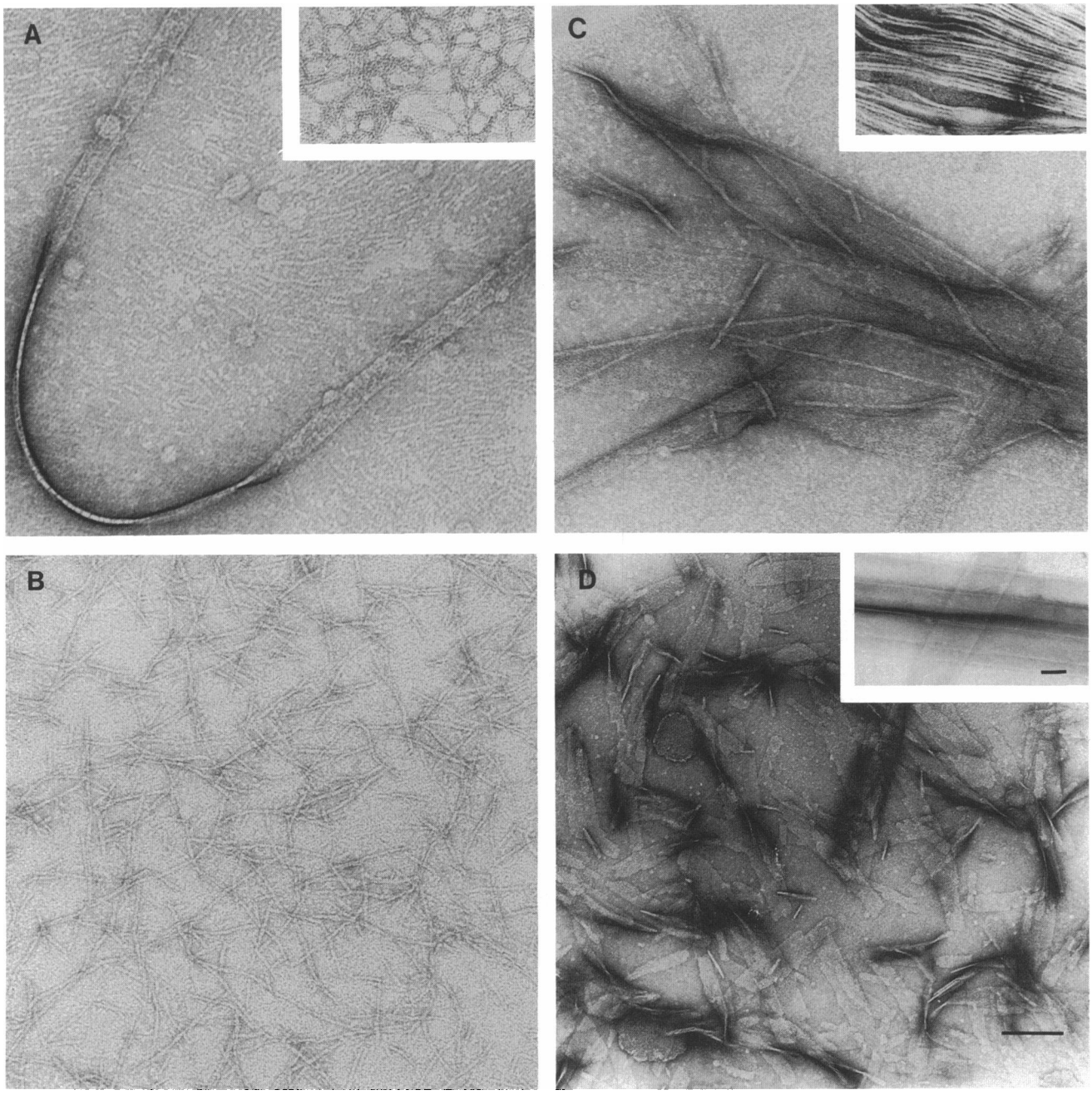

FIGURE 3 Electron micrographs of negative-stained preparations of (*A*) β-(15–28) ribbons at pH 2.0 (20 mM glycine); (*A, inset*) the fibrils observed initially at pH 2.0 before ribbon formation. (*B*) β-(15–28) at pH 7 (20 mM HEPES). (*C*) β-(17–28) ribbons formed at pH 2.0; (*C, inset*) occasional edgewise stacking of the ribbons. (*D*) β-(17–28) fragmented ribbons at pH 6.0 showing flat and edge-on views; (*D, inset*) conversion of fragments to extensive flat sheets in 500 mM NaCl. Peptide concentrations were typically 0.5–2.0 mg/ml. Scale bars, 1,000 Å.

showed the paired filaments that define the edges of the 80–100-Å fibril. A granular substructure along the filament is also evident. In cross-section, these filaments are arranged as penta- or hexamers to produce a hollow rod-like structure 110–125 Å in diameter (Fig. 5 *B*). Similar substructure and hexameric filament arrangements have also been reported for peptides derived from other regions of β/A4 (Fraser et al., 1991).

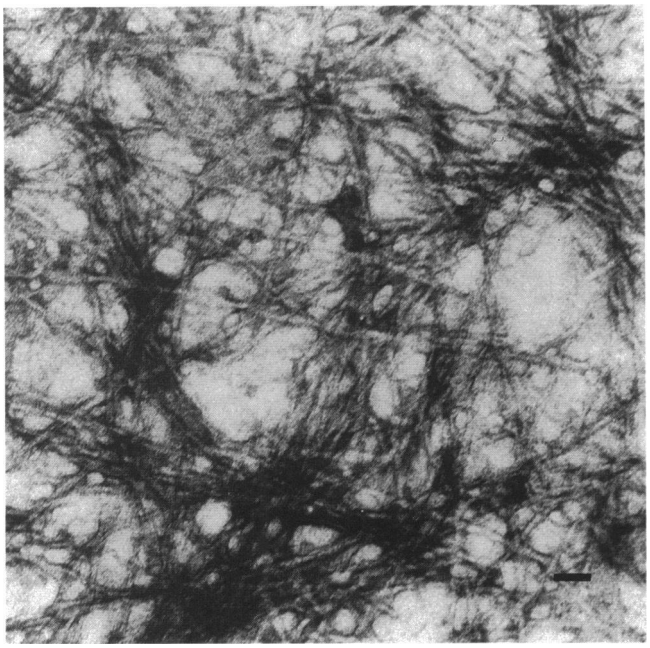

FIGURE 4 Electron micrograph of a negative-stained preparation of β-(19–28) at pH 2.0 (50 mM glycine). Peptide concentration was 20–25 mg/ml. Scale bar, 500 Å.

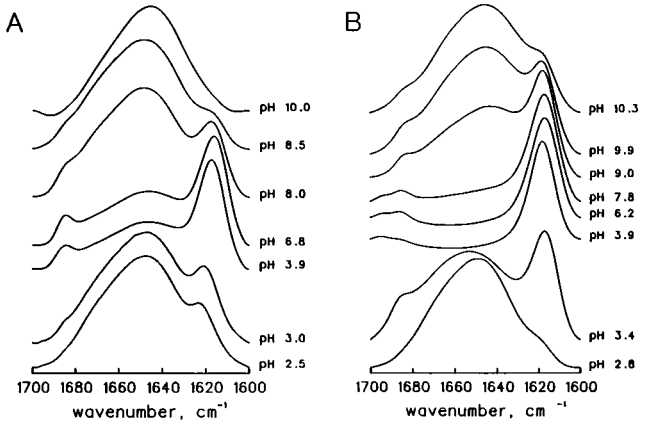

FIGURE 6 Infrared spectra of (*A*) peptide β-(1–28) and (*B*) peptide β-(9–28) indicating the pH dependence of β-structure formation. Spectra obtained for β-(11–28) and β-(13–28) were similar to those shown for β-(9–28). Adjustments to pH were made by the addition of DCl and NaOD and values were uncorrected for deuterium effects. Peptide concentrations of 3–20 mM (10–20 mg/ml) were used and did not significantly alter the appearance of the spectra.

Congo red stained assemblies were birefringent

Air-dried films of each peptide were examined for their ability to bind Congo red as well as to exhibit the diagnostic green birefringence associated with amyloid plaques, cerebrovascular amyloid, and systemic amyloid (Glenner, 1980*a*, *b*). All of the peptides bound CR as evidenced by the reddish color of the samples after staining and ethanol washing. When examined between crossed polarizers, β-(17–28) showed very weak green birefringence, while β-(15–28) and longer peptides displayed the strong birefringence typical of in situ amyloid.

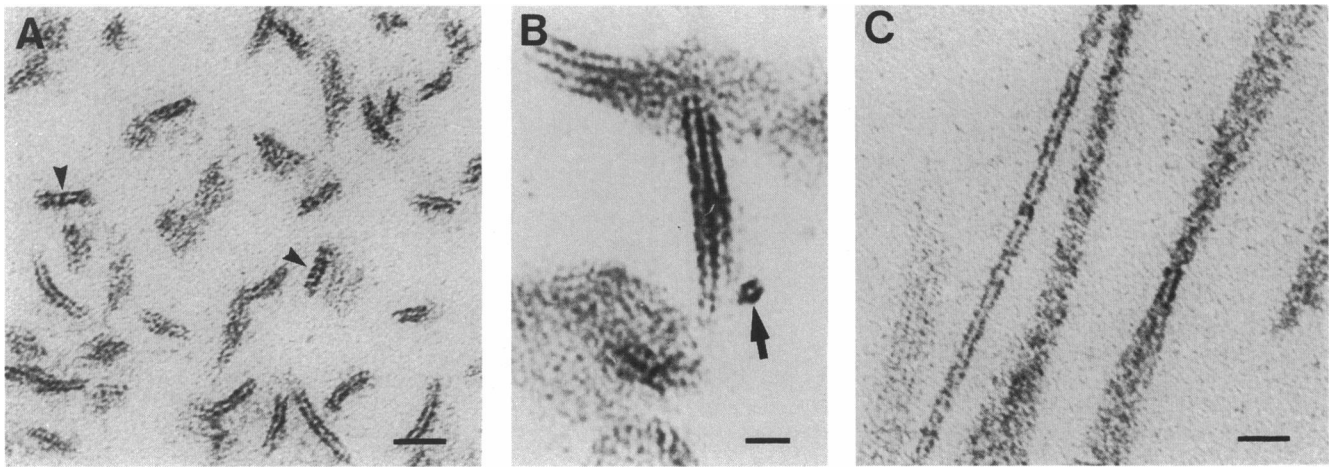

FIGURE 5 Electron micrograph of (*A*) β-(13–28) fibrils thin sectioned at an oblique angle showing the globular substructures arrayed in helical twists (*arrowheads*). (*B*) Cross-sectional view of β-(11–28) demonstrating the hollow rod structure of the fibril (*arrow*) and its penta-/hexameric arrangement of subunits; a longitudinal section of laterally aggregated fibrils is also seen. (*C*) Longitudinal section of β-(13–28) showing the paired filaments. Scale bars, 250 Å.

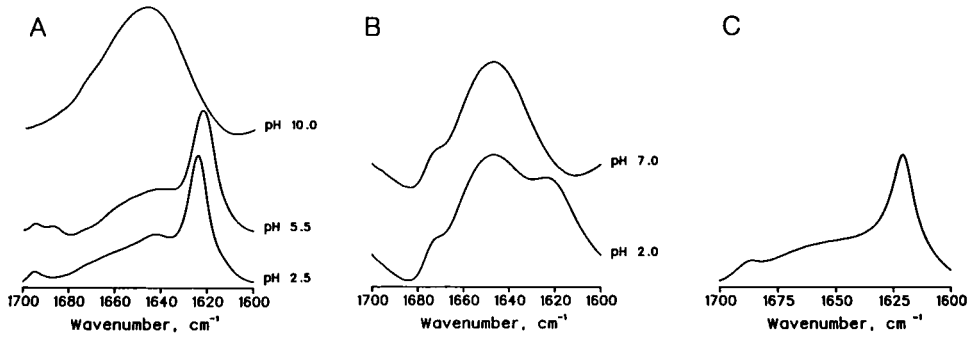

FIGURE 7 Infrared spectra of (*A*) peptide β-(15–28) indicating stable β-sheet formation at all but pH > 10 and (*B*) peptide β-(19–28) showing the mixture of random and β-conformation at pH 2. Adjustments to pH were made by the addition of DCl and NaOD and values were uncorrected for deuterium effects. Peptide concentrations were typically 10–20 mg/ml. (*C*) IR spectrum for dehydrated β-(1–28) film exhibits similar spectrum to that found in solution. Spectra obtained for remaining peptides were identical to *C* with the exception of minor frequency changes.

Previous investigations (Castano et al., 1986) have reported similar tinctorial properties of β-(1–28) and β-(12–28).

FT-IR spectroscopy indicated pH-dependent β-conformation

Proteins and peptide secondary structures display signature IR bands as a consequence of the polypeptide backbone amide bond arrangements (Surewicz and Mantsch, 1988). For example, β-pleated sheets exhibit major amide I bands at 1620–1640 cm^{-1} as compared with α-helices and random conformations with absorption at 1650–1658 cm^{-1} and 1640–1648 cm^{-1}, respectively. We have used this technique to correlate conformational transitions with peptide self assembly as a function of pH.

The spectra obtained for β-(1–28) showed β-sheet formation at pH values where fibrils were observed by

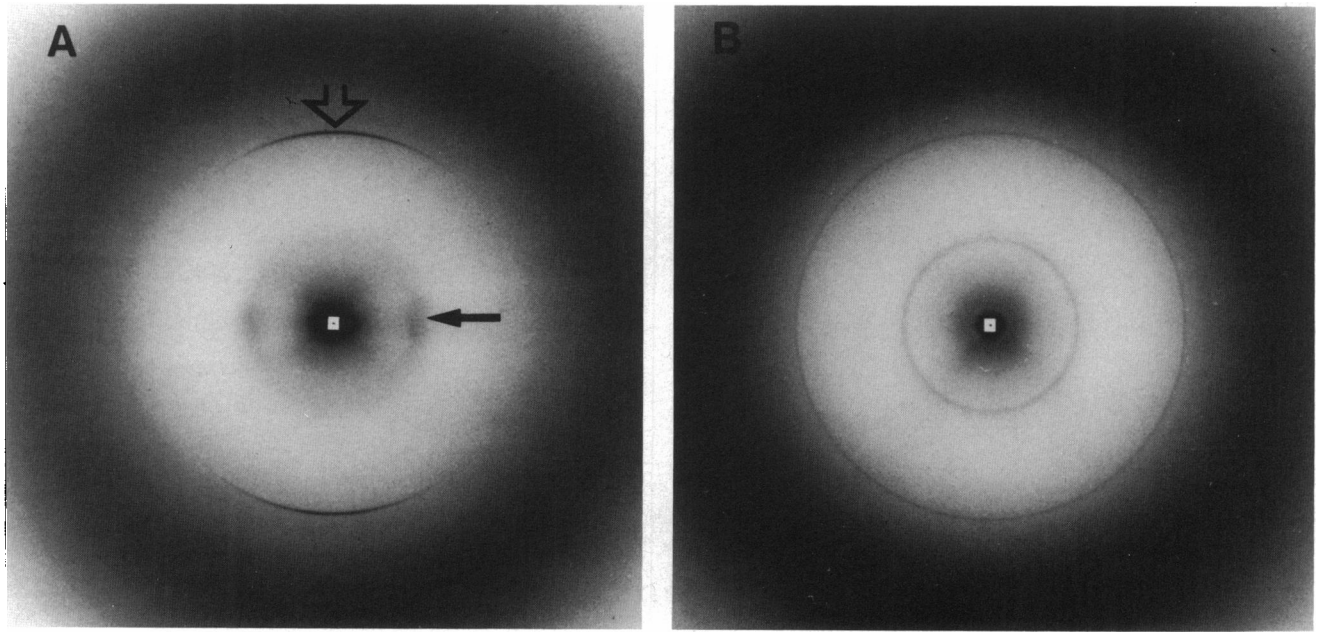

FIGURE 8 X-ray diffraction patterns of (*A*) β-(1–28), pH 5.5 (25 mM HEPES; final concentration), and (*B*) β-(17–28), pH 2.0 (25 mM glycine; final concentration). The cross-β conformation of β-(1–28) is revealed by the orthogonal positions (in *A*) of the hydrogen-bonding 4.7 Å (*open arrow*) and intersheet ~ 10 Å (*solid arrow*) reflections. Similar patterns were observed for β-(9–28), β-(11–28) and β-(13–28). Rings similar to those in *B* were observed for both β-(15–28), β-(17–28), and β-(19–28). Peptide-buffer mixtures were concentrated by drying in siliconized thin-walled glass x-ray capillaries. Final peptide concentrations were typically 30–50 mg/ml.

EM (Fig. 6 *A*). At pH 2.5 only a small β-sheet intensity at ~1620 cm^{-1} was observed and incremental pH increases resulted in progressively greater amounts of β-sheet, as indicated by the intensity of the band at 1617–1620 cm^{-1}, to a maximum of ~70–80% (as calculated from integrated intensities over the pH range of 4–7). Beyond this point the amount of β-conformation began to diminish until the peptides assumed an essentially random conformation above pH 8.5. The only ionizable groups within the β-(1–28) peptide that correspond to these particular pH values are the histidine imidazole (pK ~ 6.6) and the carboxylic acids of glutamate and aspartate (pK ~ 3). Therefore, the formation of β-sheets is optimal when these groups maintain their respective positive and negative charges.

Peptide β-(9–28) exhibited a similar relationship of β-sheet formation at low pH having appreciable intensity at 1620 cm^{-1} only above pH 3 (Fig. 6 *B*). However, the resulting β-structure persisted at much higher pH with considerable intensity remaining even at pH 9. Loss of the β-conformation only occurred above pH 10. Continued deletion of NH_2-terminal residues leading to β-(11–28) and β-(13–28) produced no effect on the ability of the peptides to form β-sheets and the IR spectra were virtually identical to those seen for β-(9–28). The morphological changes seen at higher pH values (i.e., conversion from fibers to ribbons) was not accompanied by any major frequency shifts of the β-band maxima.

β-(15–28) and β-(17–28) behaved like each other, but differed from the previous peptides in that considerable β-structure was present even at pH 2 (Fig. 7 *A*). This conformation was maintained without change at higher pH and eventually converted to a random structure only at pH 10 and greater.

The apparent lability of β-(19–28) fibrils based on electron microscopy was substantiated by FT-IR which indicated a small amount of β-sheet at low pH (Fig. 7 *B*). A considerable quantity of the peptide persisted in a random conformation suggesting an equilibrium between the aggregated and monomeric states. Any increase above pH 3 resulted in a shift of this equilibrium to an exclusively random conformation.

Dehydrated peptide assemblies exhibited β-conformation

To test whether the conformations observed by FT-IR are comparable to those found in the samples used for EM and x-ray diffraction, air-dried samples of each of the peptides were obtained. As shown in Fig. 7 *C*, the spectrum obtained for dehydrated β-(1–28) was identical to the solution spectrum, indicating little change in the fiber conformation upon drying. Similar spectra for the remaining peptides were observed with the exception that the β-maxima was shifted slightly to ~1625 cm^{-1} which may indicate a marginally weaker hydrogen bonding. β-(19–28) showed greater β-band intensity and a decrease in the random structure, suggesting that removal of water favored fiber formation. β-(19–28) exhibited the highest frequency β-band (1631 cm^{-1}) of all the peptides.

X-ray diffraction demonstrated cross-β conformation

One of the distinguishing characteristics of amyloid (cerebral and systemic) is the cross-β arrangement of the polypeptide β-sheets (Glenner, 1980). That is, the fiber axis corresponds to the hydrogen bonding (4.7 Å) direction, and the intersheet spacing at 10 Å is orthogonal to the hydrogen bonding (Geddes et al., 1968). When viewed along the appropriate axis, singly-oriented fibrils resulting from drying or sedimentation, and doubly-oriented fibrils aligned by an external force (e.g., magnetic field) show x-ray diffraction patterns (see Fraser et al., 1991), where the 4.7 Å reflection is on the meridian and the intersheet and residue repeat spacings are along the equator.

Magnetically-oriented gels of β-(1–28) (50 mg/ml) at pH 5.5 produced the diffraction pattern shown in Fig. 8 *A*. The clear distinction between the hydrogen-bonding spacing (4.7 Å) and the intersheet (10 Å) reflection indicates a cross-β conformation. The coherence lengths for the diffracting unit, calculated from the integral widths of the reflections, was several hundred Ångstroms in the H-bonding direction and 50–60 Å in the intersheet direction. The absence of any sharp small-angle equatorial spacing indicates that the fibrils were not closely packed at this concentration. However, the strong equatorial scatter at ~40 Å is suggestive of the strong, sharp reflection that is detected in dried samples (Kirschner et al., 1987). The absence of a reflection at 3.3 Å, corresponding to the repeat along the polypeptide chain, is probably accounted for by the low peptide concentration and the competing intensity produced by the excess water present in the sample. As the concentration increased to 75 and 100 mg/ml, the diffraction pattern remained unchanged.

β-(1–28) prepared at pH 9 did not appear to produce any appreciable β-structure at comparable concentrations (~50 mg/ml). This was evidenced not only by the lack of coherent diffraction but also by the absence of sample birefringence. Only at high concentration (> 100 mg/ml) did the peptide begin to show a small amount of birefringence and then only at the air–water interface.

Samples of β-(9–28), β-(11–28), and β-(13–28) at pH 5.5 and pH 9 and concentrations of 40–50 mg/ml

produced cross-β diffraction patterns similar to that of β-(1–28). The observed morphological change (from fiber to ribbon) at pH 9 was not accompanied by any corresponding change in the orientation of hydrogen-bonding relative to the long axis of the assembly (e.g., transition from cross- to extended-β). Negative staining of dispersed x-ray samples demonstrated that the ribbon structures were clearly the predominant feature of the peptide assemblies and that concentration effects were not significant.

Efforts to determine the β-sheet arrangement of β-(15–28) and β-(17–28) were complicated by problems of insolubility. β-(15–28) at all pH values appeared to be initially soluble but upon standing developed intensely birefringent domains surrounded by excess water. β-(17–28) was initially insoluble at pH <10, and after several hours of hydration a birefringent gel was observed. Diffraction from these samples gave unoriented β-sheet patterns (Fig. 8 *B*). The sharp hydrogen bonding and intersheet spacings indicates that the assemblies must be greatly extended in both H-bonding and pleated-sheet stacking directions. Coherence lengths were $\approx 1{,}000$ Å in the H-bonding directions and about one-tenth this in the intersheet direction. These dimensions are consistent with the slab-like morphology of these peptide assemblies. The gels of β-(15–28) did not become oriented in an external magnetic field. Similar unoriented patterns were obtained for β-(19–28) at pH 2.5. It was not possible, therefore, to determine if the peptides were arranged in a cross-β or extended-β motif. Other studies in our laboratory, carried out in parallel on dried samples, did however demonstrate a cross-β conformation for these peptides (Kirschner et al., 1990).

TABLE 1 Summary of principal observations

Peptide	CR	pH	FT-IR	XRD	Morphology
β-(1–28)	+	<3	R/β	ND	Fibril fragments
		3–7.5	β	x-β	Numerous amyloid-like fibrils
		>8	R	—	No fibrils
β-(9–28), (11–28), (13–28)	+	<3	R/β	ND	Small ~35 Å-diameter fibrils
		3–9	β	x-β	Numerous amyloid-like fibrils
		9	β	x-β	Ribbons 200 Å by 50 Å
		10	R	ND	No fibrils
β-(15–28)	+	<3	β	β*	Ribbons 200 Å by 50 Å
		3–9	β	β*	Ribbons/amyloid-like fibrils
		10	R	—	No fibrils
β-(17–28)	±	<3	β	β‡	Ribbons ~1,500 Å by ~80 Å
		3–9	β	ND	Ribbon fragments
		10	R	—	No fibrils
β-(19–28)	–	<3	R/β	β*	Amyloid-like fibrils ~100 Å
		>3	R	—	No fibrils

CR, Congo red birefringence, FT-IR, Fourier transform infrared spectroscopy; *XRD*, x-ray diffraction; x-β, cross-β structure; β, β-conformation; *R*, random structure; R/β, predominantly random with minor β-sheet intensity; ND, not determined; —, no structure observed. *Some cross-β conformation when dried. ‡Possibly a twisted, extended-β conformation.

DISCUSSION

β/A4 contains a number of residues with ionizable and hydrophobic sidechains that may provide the intersheet interactions necessary to form and stabilize the amyloid fibrils (Fraser et al., 1991). The pH dependence of fibril formation may yield clues concerning which residues are involved in fibrilogenesis. To explore this possibility we examined a number of peptides corresponding to truncated β/A4 sequences so that residue-specific contributions could be evaluated. Peptides included: β-(1–28), β-(9–28), β-(11–28), β-(13–28), β-(15–28), β-(17–28), and β-(19–28). These β/A4 fragments were assessed for their ability to assemble into structures that satisfied both conformational and morphological criteria (Table I). To minimize the possible conformation–constraining effects of dehydration, peptides were studied whenever possible in the presence of excess water.

The complete extracellular region of β/A4, i.e., β-(1–28), formed cross-β fibrils between pH 3–8, but was essentially random coil outside this range. Thus, fibers are formed only when the His imidazole (residues 6, 13, and 14) and the Asp/Glu carboxylic acid sidechains (residues 1, 3, 7, 11, 22, and 23) are ionized. Two possibilities may explain the pH-dependent β-sheet/fibril formation: (*a*) fibrilogenesis is dependent on one or more His-Asp/Glu salt bridges; or (*b*) peptide aggregation into fibrils is an isoelectric phenomenon as β-(1–28) is electrically neutral at pH 3–8 (i.e., 6 Asp/Glu balanced by 3 Lys/Arg and 3 His residues). While the persistence of β-structure at pH 8 argues against His (pK ~6.6) involvement, the formation of a salt bridge may result in a shift of the pK to more basic values. To test this possibility, different domains of the β-(1–28) sequence were examined. The solution behavior of these peptides pointed to several key electrostatic and hydrophobic interactions within the resulting fibrils.

The smallest peptide, β-(19–28), corresponding to the COOH-terminal region of β-(1–28), formed fibrils only at low pH that were very unstable. Peptide length and fibril instability do not necessarily correlate, as peptides

of comparable length or shorter have been shown to assemble into fibrils of considerable stability (Halverson et al., 1990). Conformational lability was echoed by the FT-IR measurements, which revealed a largely random conformation accompanied by small amounts of β-structure only at pH <3. Transition from monomers to a β-conformation was coincident with neutralization of the Glu-22 and Asp-23. It is possible that at low pH the hydrophobic NH_2-terminal residues (Phe-19; −20 and Ala-21) can participate in intersheet assembly as a consequence of reduced electrostatic repulsion between their flanking sidechains.

The importance of hydrophobic residues was confirmed with the addition of Leu-17 and Val-18, in β-(17–28), resulting in the formation of highly stable fibrils. The relative insensitivity of these fibrils to pH changes indicates that ionizable groups within β-(17–28) do not enhance intersheet interactions. No appreciable difference was observed by FT-IR after the addition of Gln-15 and Lys-16 with respect to the relationship of β-sheet formation and pH even though a charged residue is present. Although the cluster of hydrophobicity formed by the sequence Leu_{17}-Val_{18}-Phe_{19}-Phe_{20}-Val_{21} is important in promoting β-fibrils, the flat ribbon structures observed do not morphologically resemble AD amyloid. Thus, additional factors must contribute to the observed amyloid structure.

Morphology and cross-β conformation indistinguishable from that of β/A4 and β-(1–28) were achieved with the addition of two centrally-located His residues (positions 13 and 14). This type of assembly was not affected by further sequence extension to β-(11–28) and β-(9–28), including electrostatic changes produced by Glu-11. By undergoing a structural transition to ribbons at high pH these peptides did differ from β-(1–28).

The ribbons formed by β-(9–28), β-(11–28), and β-(13–28) likely result from a transition from His-Asp pairing to hydrophobic intersheet interactions in β-(15–28) and β-(17–28). Such a change in residue–residue interactions may result in increased β-strand or β-sheet twisting to relieve the strain of the unpaired Asp and Glu sidechains. This more 'open' conformation could allow for increased lateral association of filaments to produce ribbon structures. The lack of a similar morphological transition by β-(1–28) probably stems from the electrostatic repulsion created by the NH_2-terminal residues that are absent in the truncated peptides. That is, with the addition of more and more residues, β-(1–28) and probably also native amyloid with 39–42 residues become restricted to a single type of molecular organization.

Conclusions drawn from the solution conformation of the peptides assume that in vitro fibrils are comparable in behavior and structure to native AD amyloid. This assumption appears justified based on: (*a*) electron microscopy, which shows identical fibril morphology in both negative stain and high resolution thin sections (e.g., penta-/hexamerically-arranged globular subunits); (*b*) x-ray diffraction, which demonstrates a cross-β arrangement of the β-sheets; (*c*) Congo red 'apple green' birefringence; (*d*) stability under denaturing conditions; and (*e*) the observation that isolated amyloid exhibits an identical His-dependent polymerization (Masters et al., 1985*b*). Using different pH buffers, Masters et al. (1985*b*) found that higher order polymers of β/A4 (dimers and tetramers) were only observed when His residues were in their ionized form.

Several models can account for both the putative hydrophobic interactions within the sequence Leu_{17}-Val_{18}-Phe_{19}-Phe_{20}-Ala_{21} plus the His-Asp/Glu salt bridges, and the most likely is one that we have previously proposed (Kirschner et al., 1987). This entails a central intersheet core of electrostatic and hydrophobic interresidue interactions that stabilize antiparallel β-strands defined by residues 13–23. β-turns at Gly-9 and Gly-25 may promote the propagation of the β-strands along the fibril axis, and are likely involved in the folding of the full length β/A4 polypeptide.

Such a model conforms to the notion that the amyloid fibril is an extensive polymerization of β-strands as originally proposed by Glenner and co-workers (Glenner et al., 1974). In fact, the ~35-Å filaments observed for β-(9–28) at low pH may be linear polymers of the basic structural unit. Neighboring filaments could then pack together as either pentamers or hexamers to form the completed macromolecular assembly seen in AD. This contrasts with previous models presented for AD amyloid (Gorevic et al., 1987) and some systemic amyloid proteins (Turnell et al., 1986), which contain appreciable quantities of α-helix. For example, Turnell et al. (1986) proposed a subunit structure for the systemic AA amyloid combining strong hydrophobic interactions between core helices coupled with weaker hydrogen-bonding interactions between β-sheets. While this model is supported by secondary structure predictions (Turnell et al., 1986*b*), as well as CD (McCubbin et al., 1988) and FT-IR (van Andel et al., 1986) spectroscopy, it does not appear to be applicable to the AD amyloid fibrils judging from the in vitro assemblies, which are consistently in the β-conformation both in solution as a function of pH and upon drying. IR spectra of systemic amyloid are much more complex with multiple bands in the α-helix region.

One criticism of a model consisting of contiguous β-sheets is that the detailed ultrastructure of the AD amyloid fibril shows a periodic 'beading' along the fiber suggestive of globular subunits (Turnell et al., 1986*b*). Our observations of fibrils in thin section have demon-

strated identical 'globular particles' along the fiber axis (see also Fraser et al., 1991). Although there is no obvious explanation for the 'beaded' structure seen within the positively-stained fibrils, it may be the result of fixation and/or staining artifacts. X-ray measurements on samples during processing for EM could resolve this question.

The secondary structure of AD amyloid may be unique compared with the systemic amyloid. In the case of AD amyloid the extensive β-sheets may be assembled from a combination of electrostatic interactions between the His and Asp/Glu residues as well as hydrophobic packing provided by the cluster of uncharged sidechains contained within residues 17–21. Whether or not this model applies to other AD-specific fibrils (e.g., the paired helical filaments of neurofibrillary tangles) is not known at present. A cross-β structure has been reported (Kirschner et al., 1986) for paired helical filaments of the NFT, but its unique protein composition may likewise result in a mixture of secondary structures. We are currently evaluating the proposed AD amyloid model by means of selective substitutions within the β/A4 sequence based on the predicted contributions of individual residues.

The research was supported by the American Health Assistance Foundation (Dr. Kirschner), National Institutes of Health grant AG-08572 (to Dr. Kirschner). Dr. Fraser is a postdoctoral fellow of the Medical Research Council of Canada. Some of the work was carried out in facilities related to the Mental Retardation Research Center of Children's Hospital, and was supported by Core grant HD-18655 from the National Institutes of Health.

Received for publication 20 February 1991 and in final form 8 July 1991.

REFERENCES

Anderton, B. H., D. Breinburg, M. J. Downes, P. J. Green, B. E. Tomlinson, J. Ulrich, J. N. Wood, and J. Kahn. 1982. Monoclonal antibodies show that neurofibrillary tangles and neurofilaments share antigenic determinants. *Nature (Lond.)*. 298:84–86.

Buxbaum, J. D., S. E. Gandy, P. Ciccetti, M. E. Ehrlich, A. J. Czernik, R. P. Fracasso, T. V. Ramabhadran, A. J. Unterbeck, and P. Greengard. 1990. Processing of Alzheimer β/A4 amyloid precursor protein: modulation by agents that regulate protein phosphorylation. *Proc. Natl. Acad. Sci. USA*. 87:6003–6006.

Castano, E. M., J. Ghiso, F. Prelli, P. D. Gorevic, A. Migheli, and B. Frangione. 1986. In vitro formation of amyloid fibrils from two synthetic peptides of different lengths homologous to Alzheimer's disease β-protein. *Biochem. Biophys. Res. Commun.* 141:782–789.

Cohen, A. S., T. Shirahama, and M. Skinner. 1982. Electron microscopy of amyloid. *In* Electron Microscopy of Proteins (Vol. 3). J. R. Harris, editor. Academic Press, London. 165–205.

Esch, F. S., P. S. Keim, E. C. Beattie, R. W. Blacher, A. R. Culwell, T. Oltersdorf, D. McClure, and P. J. Ward. 1990. Cleavage of amyloid β peptide during constitutive processing of its precursor. *Science* (Wash. DC). 248:1122–1124.

Fraser, P. E., L. K. Duffy, M. B. O'Malley, J. Nguyen, H. Inouye, and D. A. Kirschner. 1991. Morphology and antibody recognition of synthetic β-amyloid peptides. *J. Neurosci. Res.* 28:474–485.

Geddes, A. J., K. D. Parker, E. D. T. Atkins, and E. Beighton. 1968. Cross-β conformation in proteins. *J. Mol. Biol.* 32:343–358.

Glenner, G. G., E. D. Eanes, H. A. Bladen, R. P. Linke, and J. D. Termine. 1974. β-Pleated sheet fibrils: a comparison of native amyloid with synthetic protein fibrils. *J. Histochem. Cytochem.* 22:1141–1158.

Glenner, G. G. 1980. Amyloid deposits and amyloidosis. The β-fibrilloses. *N. Engl. J. Med.* 302:1283-1292.

Glenner, G. G., and C. W. Wong. 1984*a*. Alzheimer's disease: initial report of the purification and characterization of a novel cerebrovascular amyloid protein. *Biochem. Biophys. Res. Commun.* 120:885-890.

Glenner, G. G. and C. W. Wong. 1984*b*. Alzheimer's disease and Down's syndrome: sharing of a unique cerebrovascular amyloid fibril protein. *Biochem. Biophys. Res. Commun.* 122:1131–1135.

Gorevic, P. D., E. M. Castano, K. Sarma, and B. Frangione. 1987. Ten to fourteen residue peptides of Alzheimer's disease protein are sufficient for amyloid fibril formation and its characteristic X-ray diffraction pattern. *Biochem. Biophys. Res. Commun.* 147:854–862.

Halverson, K., P. E. Fraser, D. A. Kirschner, and P. T. Lansbury, Jr. 1990. Molecular determinants of amyloid deposition in Alzheimer's disease: conformational studies of synthetic β-protein fragments. *Biochemistry*. 29:2639–2644.

Kang, J., H.-G. Lemaire, A. Unterbeck, J. M. Salbaum, C. L. Masters, K.-H. Grzeschik, G. Multhaup, K. Beyreuther, and B. Müller-Hill. 1987. The precursor of Alzheimer's disease amyloid A4 protein resembles a cell-surface receptor. *Nature (Lond.)*. 325:733–736.

Kirschner, D. A., C. Abraham, and D. J. Selkoe. 1986. X-ray diffraction from intraneuronal paired helical filaments and extraneuronal amyloid fibers in Alzheimer disease indicates cross-β conformation. *Proc. Natl. Acad. Sci. USA*. 83:503–507.

Kirschner, D. A., H. Inouye, L. K. Duffy, A. Sinclair, M. Lind, and D. J. Selkoe. 1987. Synthetic peptide homologous to β protein from Alzheimer disease forms amyloid-like fibrils *in vitro*. *Proc. Natl. Acad. Sci. USA*. 84:6953–6957.

Kirschner, D. A., P. E. Fraser, J. Nguyen, H. Inouye, K. Halverson, P. T. Lansbury, and L. K. Duffy. 1990. Structure of Alzheimer amyloid peptide assemblies *in vitro*. *Trans. Am. Soc. Neurochem.* 21:112.

Kitaguchi, N., Y. Takahashi, Y. Tokushima, S. Shiojiri, and H. Ito. 1988. Novel precursor of Alzheimer's disease amyloid protein shows protease inhibitor activity. *Nature (Lond.)*. 331:530–532.

Kosik, K. S., C. L. Joachim, and D. J. Selkoe. 1986. Microtubule-associated protein tau (τ) is a major antigenic component of paired helical filaments in Alzheimer disease. *Proc. Natl. Acad. Sci. USA*. 83:4044–4048.

Masters, C. L., G. Simms, N. A. Weinman, G. Multhaup, B. L. McDonald, and K. Beyreuther. 1985*a*. Amyloid plaque core protein in Alzheimer disease and Down syndrome. *Proc. Natl. Acad. Sci. USA*. 82:4245–4249.

Masters, C. L., G. Multhaup, G. Simms, J. Pottgiesser, R. N. Martins, and K. Beyreuther. 1985*b*. Neuronal origin of a cerebral amyloid: neurofibrillary tangles of Alzheimer's disease contain the same protein as the amyloid of plaque cores and blood vessels. *EMBO (Eur. Mol. Biol. Organ.) J.* 4:2757–2763.

McCubbin, W. D., C. M. Kay, S. Narindrsorasad, and R. Kisilevsky. 1988. Circular-dichroism studies on two murine serum amyloid A proteins. *Biochem. J.* 256:775–783.

Miyakawa, T., S. Katsuragi, and K. Watanabe. 1986. Ultrastructure of amyloid fibrils in Alzheimer's disease and Down's syndrome. *In* Amyloid and Amyloidosis. T. Isobe, S. Araki, F. Uchino, S. Kito, and E. Tsubura, editors. Plenum Press, New York. 573–578.

Mori, H., J. Kondon, and Y. Ihara. 1987. Ubiquitin is a component of paired helical filaments in Alzheimer's disease. *Science* (*Wash. DC*). 235:1641–1644.

Muga, A., W. K. Surewicz, P. T. T. Wong, and H. H. Mantsch. 1990. Structural studies with the uveopathogenic peptide M derived from retinal S-antigen. *Biochemistry.* 29:2925–2930.

Palmert, M. R., M. B. Podlisny, D. S. Witker, T. Oltersdorf, L. H. Younkin, D. J. Selkoe, and S. G. Younkin. 1989. The β-amyloid protein precursor of Alzheimer disease has soluble derivatives found in human brain and cerebrospinal fluid. *Proc. Natl. Acad. Sci. USA.* 86:6338–6342.

Ponte, P., P. Gonzalez-DeWhitt, J. Schilling, J. Miller, D. Hsu, B. Greenberg, K. Davis, W. Wallace, I. Lieberburg, F. Fuller, and B. Cordell. 1988. A new A4 amyloid mRNA contains a domain homologous to serine proteinase inhibitors. *Nature* (*Lond.*). 331:525–527.

Selkoe, D. J. 1989. Biochemistry of altered brain proteins in Alzheimer's disease. *Annu. Rev. Neurosci.* 12:463–490.

Sisodia, S. S., E. H. Koo, K. Beyreuther, A. Unterbeck, and D. L. Price. 1990. Evidence that β-amyloid protein in Alzheimer's disease is not derived by normal processing. *Science* (*Wash. DC*). 248:492–495.

Spillantini, M. G., M. Goedert, R. Jakes, and A. Klug. 1990*a*. Different configurational states of β-amyloid and their distributions relative to plaques and tangles in Alzheimer disease. *Proc. Natl. Acad. Sci. USA.* 87:3947–3951.

Spillantini, M. G., M. Goedert, R. Jakes, and A. Klug. 1990*b*. Topographical relationship between β-amyloid and tau protein epitopes in tangle-bearing cells in Alzheimer disease. *Proc. Natl. Acad. Sci. USA.* 87:3952–3956.

Surewicz, W. K., and H. H. Mantsch. 1988. New insight into protein secondary structure from resolution-enhanced infrared spectra. *Biochim. Biophys. Acta.* 952:115–130.

Tanzi, R. E., A. I. McClatchey, E. D. Lamperti, L. Villa-Komaroff, J. F. Gusella, and R. L. Neve. 1988. Protease inhibitor domain encoded by an amyloid protein precursor mRNA associated with Alzheimer's disease. *Nature* (*Lond.*). 331:528–530.

Turnell, W., R. Sarra, J. O. Baum, D. Caspi, M. L. Baltz, and M. B. Pepys. 1986*a*. X-ray scattering and diffraction by wet gels of AA amyloid fibrils. *Mol. Biol. Med.* 3:409–424.

Turnell, W., R. Sarra, I. D. Glover, J. O. Baum, D. Caspi, M. L. Baltz, and M. B. Pepys. 1986*b*. Secondary structure prediction of human SAA_1: presumptive identification of calcium and lipid binding sites. *Mol. Biol. Med.* 3:387–407.

Van Andel, A. C. J., Th. A. Niewold, E. T. G. Lutz, J. H. van der Maas, P. Limburg, and E. Gruys. 1986. Fourier transform infrared spectroscopy of air-dried and heavy water suspended AA and AL amyloid fibril preparations of different species. *In* Amyloid and Amyloidosis T. Isobe, S. Araki, F. Uchino, S. Kito, and E. Tsubura, editors. Plenum Press, New York. 45–50.

Wischik, C. M., M. Novak, H. C. Thogersen, P. C. Edwards, M. J. Runswick, R. Jakes, J. E. Walker, C. Milstein, M. Roth, and A. Klug. 1988. Isolation of a fragment of tau derived from the core of the paired helical filament of Alzheimer disease. *Proc. Natl. Acad. Sci. USA.* 85:4506–4510.

Yankner, B. A., L. K. Duffy, and D. A. Kirschner. 1990. Neurotrophic and neurotoxic effects of amyloid β-protein: reversal by tachykinin neuropeptides. *Science* (*Wash. DC*). 250:279–282.